



Time-dependent adsorption and resistant desorption of arsenic on magnetite nanoparticles: kinetics and modeling

Weichun Yang^{a,*}, Na Zhao^a, Nan Zhang^c, Wei Chen^b, Amy T. Kan^c, Mason B. Tomson^c

^a*School of Metallurgical Science and Engineering, Central South University, Changsha Hunan 410083, China
Tel. + 86 731 88830875; Fax. + 86 731 88710171; email: yang220222000@yahoo.com.cn*

^b*College of Environmental Science and Engineering, Nankai University, Tianjin 300071, China*

^c*Department of Civil and Environmental Engineering, Rice University, Houston, TX 77005, USA*

Received 18 April 2011; Accepted 8 December 2011

ABSTRACT

Arsenic contamination in water is a worldwide problem and poses a significant challenge for the environmental engineers. Magnetite nanoparticles are a highly promising adsorbent for the effective removal of arsenic from drinking water. In the present study, an arsenic adsorption kinetic study was carried out on magnetite nanoparticles at pH 8.0 (a typical pH for groundwater), followed by sequential desorption with arsenic-free background solution. The results illustrate that arsenic adsorption on magnetite nanoparticles is nonlinear and time-dependent. The adsorption kinetics of both As(V) and As(III) are biphasic, where the arsenic adsorption is rapid initially and is followed by a slower adsorption with increasing reaction time. Desorption of both As(V) and As(III) exhibited clear hysteresis, a considerable amount of arsenic is resistant to desorption. Freundlich model, diffusion layer model (DLM), biphasic first-order kinetic model were used to fit the arsenic adsorption on magnetite nanoparticles and multi-reaction model (MRM) was used to describe the adsorption and desorption of arsenic on magnetite nanoparticles. Surprisingly, both of the observed arsenic adsorption and desorption kinetics can be fitted with MRM model very well, indicating that MRM model is potentially useful in modeling fate of arsenic in water treatment with magnetite nanoparticles. This work is important in offering insight into the adsorption mechanism of arsenic from magnetite nanoparticles and predicting the fate of arsenic in magnetite nanoparticle-based water treatment.

Keywords: Arsenic; Biphasic adsorption; Resistant desorption; Multi-reaction model; Magnetite nanoparticles; oxidation

1. Introduction

Arsenic contamination in water has become a worldwide problem due to its significant threat to human health. It is reported that over 137 million people in more than 70 countries are affected by arsenic poisoning of drinking water [1]. Arsenic removal via adsorption is one of the most common methods used in water treatment.

Recently, arsenic removal using nano-scale iron oxides has received considerable attention [2–5]. It has been found that magnetite nanoparticles are a highly promising adsorbent for arsenic removal from drinking water [3,6–8]. Besides having high affinities for both As(III) and As(V), magnetite nanoparticles can be easily separated after treatment using low-field magnets or by simple filtration. Thus far, adsorption and desorption of arsenic on magnetite nanoparticles have not been studied systematically, and a thorough understanding of these

*Corresponding author.

processes is critical for the development of magnetite nanoparticle-based arsenic removal in water treatment.

Adsorption kinetics is one of the most important factors affecting the practical use of arsenic removal with magnetite nanoparticles, in that it can greatly affect the removal efficiency. It has been reported that adsorption of arsenic to iron oxides is a two-step process, consisting an initial rapid phase followed by a much slower phase [9–15]. The proposed mechanisms accounting for the slow adsorption phase include interparticle/intraparticle diffusion, surface precipitation, heterogeneity of adsorption sites, and formation of a solid-solution on the surface [12,16,17]. Fuller et al. [9] observed a period of rapid (<5 min) arsenate adsorption to ferrihydrite followed by continued adsorption for at least 8 d. They attributed the rate-limiting arsenate adsorption step to slow diffusion to adsorption sites within aggregates of ferrihydrite. Similar mechanism was also proposed by Raven et al. [10] and Luengo et al. [18] to explain the slow arsenic adsorption to ferrihydrite and goethite. Zhang and Stanforth [14] argued that the slow stage of As(V) adsorption to goethite is most likely due to the heterogeneity of the surface site bonding energy rather than the diffusion processes. Thus far, very little information is available on the adsorption kinetics of arsenic to magnetite nanoparticles.

Understanding of the desorption process of arsenic from magnetite nanoparticles is not only important for the regeneration of spent magnetite nanoparticles, but also critical to the assessment of the safety of this technology. For example, if the extent of desorption of arsenic from magnetite nanoparticles is very low, there can be little concern on the re-release of arsenic from magnetite nanoparticle after its adsorption. Several studies have been conducted to characterize the desorption of arsenic from iron oxides or soils [19–22]. Lin and Puls [19] reported hysteretic desorption of As(III) and As(V) from clay minerals, and proposed that during the aging process arsenic can diffuse into the internal pores of the clay aggregates or the dehydration of adsorbed arsenic, which can lead to enhanced bonding of arsenic to clays. Genç-Fuhrman et al. [23] found that desorption of As(V) from activated red mud was very low (only ≈40% desorbed) when pH was raised to 11.6, due to chemisorption. Yean et al. [6] observed the desorption of arsenite and arsenate on magnetite nanoparticles was hysteretic, and presumed that the binding of the adsorbed arsenic resulted in the formation of highly stable iron-arsenic complexes uniformly over the surface.

In the present study, we evaluated the time-dependent adsorption and desorption of arsenic on magnetite nanoparticles. The adsorption and desorption data were compared with the predictions of several common adsorption/desorption models. Mechanisms controlling

arsenic adsorption/desorption to magnetite nanoparticles are also discussed.

2. Materials and methods

2.1. Materials

As(III) oxide (As_2O_3) and As(V) oxide hydrate ($\text{As}_2\text{O}_5 \cdot 3\text{H}_2\text{O}$) were purchased from Sigma Aldrich (St. Louis, MO, USA). Stock solutions of As(III) and As(V) were prepared by dissolving a certain amount of As_2O_3 or $\text{As}_2\text{O}_5 \cdot 3\text{H}_2\text{O}$ in 0.1 mol l^{-1} NaOH. Aqueous solutions were prepared in an electrolyte solution containing 0.01 mol l^{-1} NaNO_3 and 0.005 mol l^{-1} Tris buffer at pH 8.0, and pH was adjusted with 6 mol l^{-1} HNO_3 or 1 mol l^{-1} NaOH.

Magnetite nanoparticles were obtained from Reade Advanced Materials (Reno, NV, USA). The BET surface area ($60 \text{ m}^2 \text{ g}^{-1}$), nominal particle size (19.3 nm), and point of zero charge (pHpzc) (6.8) have been reported in a previous paper [6].

2.2. Adsorption isotherms

Adsorption isotherms were obtained using a batch adsorption approach. First, 6 mg of magnetite nanoparticles was added to a series of 60 ml polypropylene vials. The vials were filled with an aqueous solution of As(III) or As(V), and were equilibrated end-over-end (4 rpm) for 15 h. Afterwards, the vials were centrifuged at 4000 rpm for 30 min, and the pH of the supernatant was measured. A portion of the supernatant was withdrawn and filtered through a $0.45 \mu\text{m}$ membrane filter (Millipore, Billerica, MA, USA) with a disposable syringe. Iron in the filtrate was checked for selected samples to verify that the filter could sufficiently retain the magnetite nanoparticles, and Fe was not detected in any samples. The filtered samples were then acidified with 1% nitric acid (V/V) for sample preservation prior to arsenic analysis. The amount of adsorbed As(III)/As(V) was calculated from the measured solution-phase concentration based on mass balance. Additional time-dependent adsorption isotherms of As(III) (at 24, 48, 72 and 120 h) were obtained using the same procedures mentioned above.

2.3. Desorption isotherms

Selected vials from the 15 h As(III) and As(V) adsorption experiments were used in desorption experiments. Repetitive desorption data was obtained by successively replacing about 90% of the supernatant with arsenic-free aqueous solution. The equilibration time for each repetitive desorption step was 24 h, and were equilibrated end-over-end (4 rpm). At the end of each desorption step, the vial was centrifuged at 4000 rpm for 30 min,

and the supernatant was withdrawn. A portion of the supernatant was taken to analyze the aqueous arsenic concentration, and the arsenic-free solution was added to initiate the next desorption step. After the last desorption step, two reaction vials from the As(V) desorption experiment were used to check arsenic mass balance by digestion with concentrated nitric acid at 95°C for 24 h. The mass balance was found to be 98.1% and 100.7% for the two samples.

2.4. Adsorption kinetics

Adsorption kinetics experiments were carried out in 60 ml polypropylene vials with two initial concentrations for both As(III) (234 and 572 $\mu\text{g l}^{-1}$) and As(V) (285 and 695 $\mu\text{g l}^{-1}$), using the same procedures in adsorption isotherm experiments. For each input concentration, 1 ml aliquots of the suspension were collected at selected time intervals and filtered through a 0.22 μm membrane filter for arsenic analysis.

To examine the effect of redox on arsenic adsorption on magnetite nanoparticles, adsorption kinetic experiments were carried out in 1 l glass container under aerated condition and deoxygenated condition controlled by continuous purging with argon gas. In the aerated experiment, about 1000 ml aqueous solution of 100 $\mu\text{g l}^{-1}$ arsenic was added to the glass container. Then, 0.1 g magnetite nanoparticles was added to the solution exposed to atmosphere. In the experiments involving deoxygenated condition, the arsenic solution was sparged with argon gas for 20 min prior to the addition of magnetite nanoparticles, and argon sparging was continued throughout the duration of the experiment. Afterwards, the suspension was agitated using an overhead propeller electric stirrer (Arrow Engineering, Hillside, NJ, USA). At selected time intervals, 10 ml aliquots of the suspension were collected and filtered for arsenic analysis. The pH of the suspension was measured at the end of each experiment.

2.5. Analytical methods

Arsenic was measured at 74.921 m e^{-1} with a Perkin Elmer Elan 9000 ICP-MS (Atlanta, GA, USA). ICP-MS was calibrated at 0–100 $\mu\text{g l}^{-1}$ with arsenic standard solutions in four-to-five-point calibration. Germanium (Ge) was used as the internal standard for calibration. Excellent linear calibration was generally observed with correlation of 0.9999 or better. A quality control sample was analyzed every six samples to ensure that the calibration was valid for the analysis. The detection limit for arsenic was 0.02 $\mu\text{g l}^{-1}$ for ICP-MS and the relative standard deviation of three replicate analyses was generally below 3%.

3. Calculation

3.1. Freundlich adsorption model

The Freundlich model is expressed as:

$$q = K_F \cdot C^N \quad (1)$$

where q ($\mu\text{g kg}^{-1}$) and C ($\mu\text{g l}^{-1}$) represent the concentrations of adsorbed arsenic and aqueous arsenic respectively; K_F is the Freundlich affinity coefficient ($\mu\text{g}^{1-N} \cdot \text{l}^N \cdot \text{kg}^{-1}$) and N (unitless) is the Freundlich linearity index.

3.2. Biphasic first-order kinetic model

Adsorption kinetics of arsenic by magnetite nanoparticles was fitted with a biphasic first-order kinetic model:

$$(C_t - C_e) / (C_0 - C_e) = f \cdot e^{-k_r \cdot t} + (1 - f) \cdot e^{-k_s \cdot t} \quad (2)$$

where C_t ($\mu\text{g l}^{-1}$) is the solution phase arsenic concentration at a given time; C_e ($\mu\text{g l}^{-1}$) is arsenic concentration at adsorption equilibrium; C_0 ($\mu\text{g l}^{-1}$) is the initial arsenic concentration; t (h) is the reaction time; k_r (h^{-1}) and k_s (h^{-1}) are the apparent first-order rate constants for the rapid and slow adsorption fractions, respectively; and f is the mass fraction associated with the slow adsorption fraction. This four-parameter biphasic first-order adsorption model is an empirical model, and its parameters are useful to distinguish rapidly and slowly adsorption fractions. The nonlinear least-square optimization program (Sigma-Plot 10.0) was used to obtain the best-fit parameters.

3.3. Diffusion layer model

DLM, one of the most commonly used surface complexation models (SCMs), was also used to model arsenic adsorption on magnetite nanoparticles, accounting for the specific chemical and electrostatic interactions occurring at the surface. This model assigns two layers in the interfacial region: a surface layer containing a fixed charge and a diffuse layer of counterions, opposite charge to fixed charge in solution. The relationship between surface charge and the potential is generalized by the Gouy–Chapman theory [24]. Similar to other commonly used SCMs, DLM has often been used to describe arsenic adsorption to iron oxides and is capable of addressing pH effects and electrostatic contributions to adsorption. The adsorption reaction constants were obtained by fitting model-calculated values using the chemical speciation program Visual MINTEQ [25].

3.4. Multi-reaction model

An MRM was used to model the time-dependent adsorption of arsenic on magnetite nanoparticles.

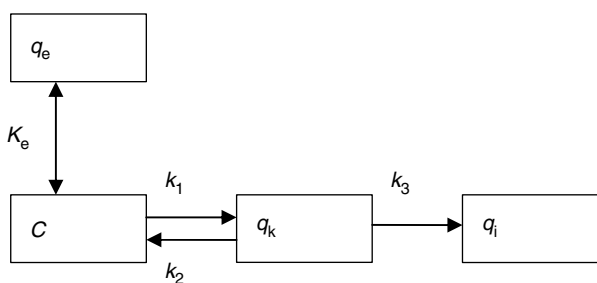


Fig. 1. Schematic of the MRM for arsenic on magnetite nanoparticles. C represents solution concentration, q_e , q_k and q_i represent the amounts sorbed at equilibrium, kinetic, and irreversible sites, respectively, and K_e is a Freundlich-type dimensionless equilibrium constant, k_1 , k_2 and k_3 are the respective reaction rate constants.

The MRM is similar to the literature models used to describe the time-dependent adsorption of heavy metals to soils [26–28] and is based on the assumption that a fraction of the total adsorption sites reacts rapidly or instantaneously with arsenic whereas the remaining fraction of sites reacts slowly with arsenic. Fig. 1 shows the schematic illustration of the MRM, which can be described using the following mathematical formulation:

$$q_e = K_e (\theta/\rho) C^n \quad (3)$$

$$\partial q_k / \partial t = k_1 (\theta/\rho) C^n - (k_2 + k_3) q_k \quad (4)$$

$$\partial q_i / \partial t = k_3 \cdot q_k \quad (5)$$

where C ($\mu\text{g l}^{-1}$) represents solution concentration, q_e ($\mu\text{g kg}^{-1}$), q_k ($\mu\text{g kg}^{-1}$) and q_i ($\mu\text{g kg}^{-1}$) represent the mass associated with the equilibrium, kinetic, and irreversible sites, respectively, K_e ($\mu\text{g}^{1-n} \cdot \text{l}^n \cdot \text{kg}^{-1}$) is a Freundlich-type equilibrium constant, k_1 and k_2 (h^{-1}) are the forward and backward reaction rates associated with kinetics sites, respectively, k_3 (h^{-1}) is the irreversible rate coefficient associated with kinetic sites, n is the dimensionless reaction order, θ (unitless) is the water content, ρ is sorbent density (kg l^{-1}), t (h) is the reaction time. The best-fit parameters of K_e , n , k_1 , k_2 and k_3 were obtained based on Newton's method, Runge-Kutta method and non-linear least-squares optimization method [29].

4. Results and discussion

4.1. Time-dependent adsorption isotherms

Fig. 2(a) shows the time-dependent adsorption isotherms (15 h) of As(III) and As(V) on magnetite nanoparticles. Both isotherms followed the Freundlich model (Eq. (1)) well. The fitted K_F values were 49,499 for As(III)

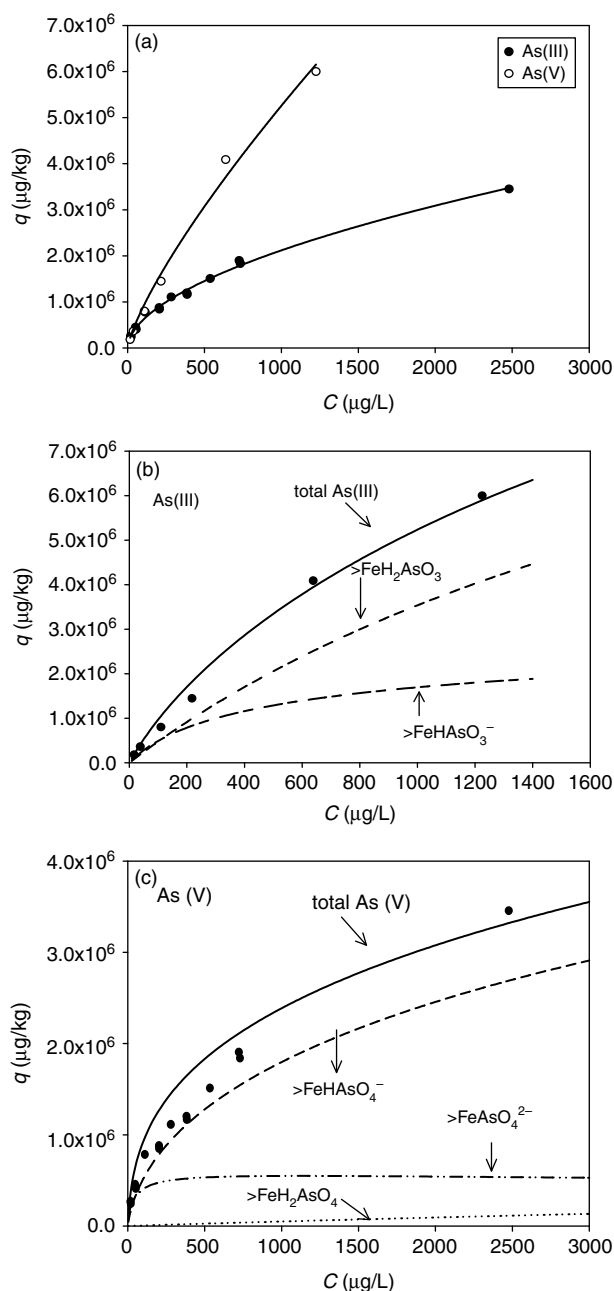


Fig. 2. (a) Adsorption isotherms of As(III) and As(V) for 15 h fitted by Freundlich model. Simulation of (b) As(III) adsorption isotherm and (c) As(V) adsorption isotherms with DLM model. Data are shown as symbols and model fits are shown as lines.

and 24,745 for As(V), and the N values were 0.7758 for As(III) and 0.5438 for As(V). As(V) exhibited less affinity for magnetite nanoparticles than As(III) at pH 8.0, especially at higher concentrations. This observation is similar to those by Morin et al. [30] using maghemite as the sorbent (pH 8–8.5) and by Dixit and Hering [31] using amorphous iron oxide and goethite as the sorbents (pH range 6–9). In the present study, the surface

of magnetite nanoparticles was negatively charged at pH 8.0; the predominant species of As(V) in the solution were HAsO_4^{2-} and H_2AsO_4^- , whereas As(III) existed predominantly as a neutral species, H_3AsO_3 . Thus, the lower adsorption of As(V) was likely due to the electrostatic repulsion between the As(V) and the surface of magnetite nanoparticles.

To incorporate the electrostatic contribution to the adsorption of arsenic on magnetite nanoparticle surface (at pH 8), the DLM was used to fit the adsorption isotherms. The model parameters, including specific surface area of the magnetite nanoparticles ($60 \text{ m}^2 \text{ g}^{-1}$), surface site density (2.2 site nm^{-2}), and the equilibrium constants for the magnetite surface, were taken from literature studies [31,32]. The constants of aqueous reaction for As(V) and As(III) were from the database of Visual MINTEQ.2.53. Table 1 provides the surface protonation and adsorption reactions along with their constants.

Figs. 2(b) and (c) show the model-fit results, indicating that DLM can describe the observed As(III) and As(V) adsorption data well. The adsorption constants for both As(III) and As(V) are similar to those reported for the adsorption of As(III) and As(V) on goethite and magnetite by Dixit and Hering [31]. Based on DLM, the As(III) adsorption might be caused by the formation of surface complex $\equiv\text{FeH}_2\text{AsO}_3$ and $\equiv\text{FeHAsO}_3^-$, where as

Table 1
Reactions and parameters used in surface complexation modeling

Surface acidity reaction	Log K^a
$\equiv\text{FeOH} + \text{H}^+ \rightarrow \equiv\text{FeOH}_2^+$	4.6
$\equiv\text{FeOH} \rightarrow \equiv\text{FeO}^- + \text{H}^+$	-8.2
Adsorption reaction for As(III)	
$\equiv\text{FeOH} + \text{H}_3\text{AsO}_3 \rightarrow \equiv\text{FeH}_2\text{AsO}_3 + \text{H}_2\text{O}$	4.42
$\equiv\text{FeOH} + \text{H}_3\text{AsO}_3 \rightarrow \equiv\text{FeHAsO}_3^- + \text{H}^+ + \text{H}_2\text{O}$	-2.50
Adsorption reaction for As(V)	
$\equiv\text{FeOH} + \text{AsO}_4^{3-} + 3\text{H}^+ \rightarrow \equiv\text{FeH}_2\text{AsO}_4 + \text{H}_2\text{O}$	30.50
$\equiv\text{FeOH} + \text{AsO}_4^{3-} + 2\text{H}^+ \rightarrow \equiv\text{FeHAsO}_4^- + \text{H}_2\text{O}$	25.79
$\equiv\text{FeOH} + \text{AsO}_4^{3-} + \text{H}^+ \rightarrow \equiv\text{FeAsO}_4^{2-} + \text{H}_2\text{O}$	19.10
Number of site types	1
Model type	Diffuse double layer model
Site density (sites/ nm^2)	2.2 ^c
Specific surface area ($\text{m}^2 \text{ g}^{-1}$)	60
Equilibration time (h)	15

^aMarmier et al. [32].

^bThis study.

^cDixit and Hering [31].

the As(V) adsorption mainly caused by the formation of surface complex $\equiv\text{FeHAsO}_4^-$ and $\equiv\text{FeAsO}_4^{2-}$.

To further understand the time-dependent adsorption properties, adsorption isotherms of As(III) focused on low concentrations ($0\text{--}220 \mu\text{g l}^{-1}$) were obtained at 15, 24, 48, 72 and 120 h. All of the adsorption isotherms followed the Freundlich model reasonably (Fig. 3(a)), and the fitted Freundlich parameters are summarized in Table 2.

In general, As(III) adsorption was increasingly nonlinear with the increase of adsorption time, the N value decreased from 0.817 to 0.398 as adsorption time increased from 15 to 120 h. The increased nonlinearity seems to indicate that the adsorption sites on magnetite nanoparticles become increasingly heterogeneous with reaction time. This might be due to oxidation occurring on magnetite surface which was redox-active, resulting in generation of many heterogeneous adsorption sites for arsenic. The time-dependent property was also evident with the increase of K_F values with time.

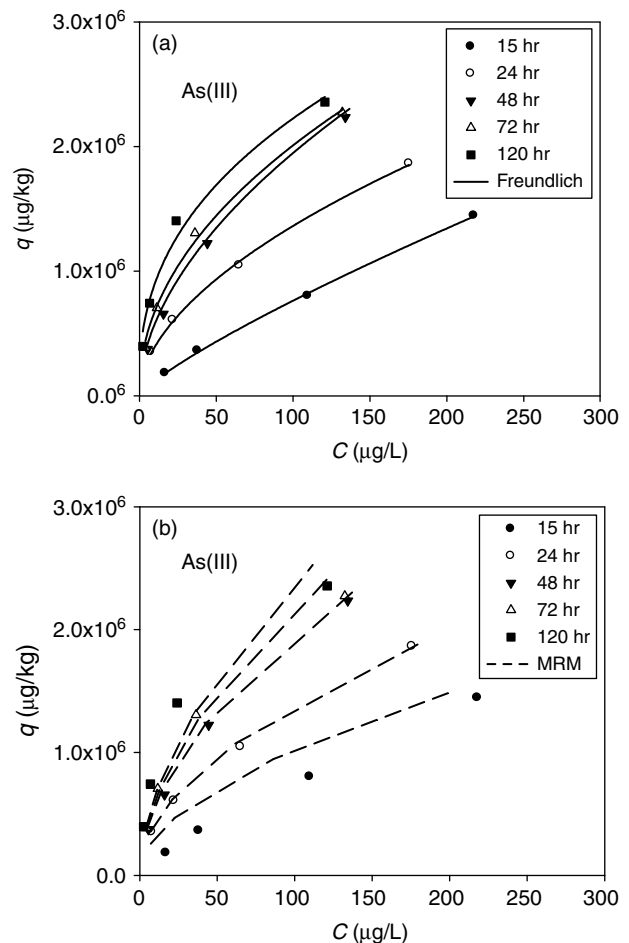


Fig. 3. Adsorption isotherms of As(III) fitted by (a) Freundlich model and (b) MRM model. Symbols are data points for different reaction time of 15, 24, 48, 72 and 120 h (from bottom to top). Lines represent model simulations.

Table 2
Parameters of Freundlich model and Multireaction model fitted to As(III) adsorption isotherms

Data set ^a	Freundlich model			Multireaction model (MRM)					
	K_F	N	r^2	n	K_e	k_1 (h ⁻¹)	k_2 (h ⁻¹)	k_3 (h ⁻¹)	r^2
15 h	17690 ± 2139	0.817 ± 0.023	0.999						
24 h	109566 ± 8615	0.547 ± 0.016	0.999	0.572 ±	2.130 ±	0.436±	0.029±	0.0016 ±	0.992
48 h	142045 ± 6388	0.563 ± 0.010	0.999	0.007	0.381	0.027	0.002	0.0004	
72 h	221931 ± 26044	0.478 ± 0.026	0.996						
120 h	355357 ± 66522	0.398 ± 0.044	0.984						

^a“data set” represents As(III) adsorption isotherms for different reaction time including 15, 24, 48, 72 and 120 h.

4.2. Adsorption kinetics

Fig. 4 shows the adsorption kinetics data of As(III) and As(V), each involving a high and a low initial concentrations in the solution. The adsorption kinetic was clearly biphasic—including an initial rapid stage and then a much slower one—and can be well described with the biphasic first-order kinetic model (Eq. 2). The fitted model parameters are listed in Table 3.

For both As(III) and As(V) approximately 31–44% of the adsorbed mass was associated with the rapid-adsorption fraction, and the k_r value was over one order of magnitude higher than the respective k_s value. Similar biphasic patterns have been observed for arsenic adsorption to mineral oxides [9,33,34] and to soils [14].

Many mechanisms (such as interparticle/intraparticle diffusion, surface precipitation, surface site heterogeneity, and formation of a solid-solution on the surface) have been proposed to interpret the slow adsorption process of arsenic to mineral oxides and soils [12,16,17]. Considering magnetite was characterized

with reducing ability, oxidation was likely one of the contributing factors to the time-dependent of arsenic adsorption on magnetite. Therefore, the effect of redox on adsorption of arsenic on magnetite nanoparticles was examined along with the adsorption kinetics under aerated and deoxygenated conditions (Fig. 5). The time-dependent adsorption results in both the aerated and deoxygenated conditions corresponded to biphasic behavior. In addition, there was no obvious effect on arsenic adsorption rate for these two conditions in the first 2 h. However, the long term adsorption of both As(V) and As(III) under deoxygenated condition was much slower than that of the aerated condition. At the end of the experiment, the amount adsorbed under deoxygenated condition was lowered by about 14% for both As(V) and As(III). The slow kinetics might be related to the degree of oxidation. Both water molecular and dissolved O₂ can be oxidants of the magnetite surface and the redox reactions of magnetite could be described by:

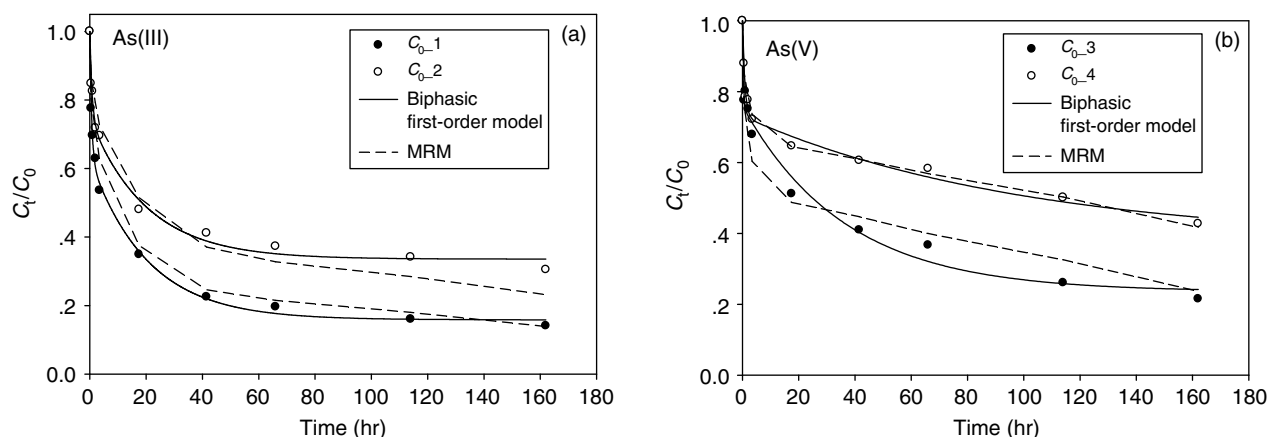


Fig. 4. (a) As(III) and (b) As(V) concentration in solution versus time during adsorption. Symbols are data points for different initial concentrations. Solid lines represent biphasic first-order model simulation, and dotted Lines represent MRM model simulation based on the parameters in Table 2 for As(III), and using the parameters optimized by data set of ‘Overall’ in Table 3 for As(V).

Table 3

Parameters of biphasic first-order kinetics and multi-reaction models to As(III) and As(V) kinetics data

Data set ^a		Biphasic first-order adsorption kinetic model					
		C_e/C_0^c	f	k_r (h ⁻¹)	k_s (h ⁻¹)	r^2	
As(III)	C _{0_1}	0.1583 ± 0.0138	0.4415 ± 0.0376	1.5020 ± 0.2887	0.0489 ± 0.0074	0.997	
	C _{0_2}	0.3356 ± 0.0191	0.3823 ± 0.0710	1.2485 ± 0.5133	0.0494 ± 0.0123	0.992	
	Deoxygenated	0.3098 ± 0.0156	0.5795 ± 0.0638	0.7534 ± 0.1426	0.0760 ± 0.0227	0.997	
	Aerated	0.1748 ± 0.0157	0.2635 ± 0.0461	6.1310 ± 2.9562	0.1698 ± 0.0218	0.996	
As(V)	C _{0_3}	0.2357 ± 0.0385	0.3145 ± 0.0695	3.5405 ± 2.5678	0.0275 ± 0.0070	0.985	
	C _{0_4}	0.3753 ± 0.0913	0.4308 ± 0.0661	1.2146 ± 0.3478	0.0100 ± 0.0052	0.989	
	Deoxygenated	0.4509 ± 0.0093	0.4807 ± 0.0457	3.5335 ± 0.7346	0.1391 ± 0.0264	0.996	
	Aerated	0.3121 ± 0.0157	0.4199 ± 0.0689	2.1105 ± 0.6506	0.1384 ± 0.0321	0.995	
Multireaction model							
		n	K_e	k_1 (h ⁻¹)	k_2 (h ⁻¹)	k_3 (h ⁻¹)	r^2
As(V)	Overall	0.455 ± 0.011	4.966 ± 0.373	1.157 ± 0.105	0.1093 ± 0.0068	0.0034 ± 0.0001	0.995

^a“C_{0_1}” and “C_{0_2}” refer to kinetic experiments initiated from As(III) concentrations of 234 and 572 μg l⁻¹, respectively; while “C_{0_3}” and “C_{0_4}” refer to kinetic experiments initiated from As(V) concentrations of 285 and 695 μg l⁻¹, respectively.

“Deoxygenated” and “Aerated” represent kinetic experiments conducted under deoxygenated and aerated conditions.

“Overall” includes the data sets of “C_{0_3}” and “C_{0_4}”.

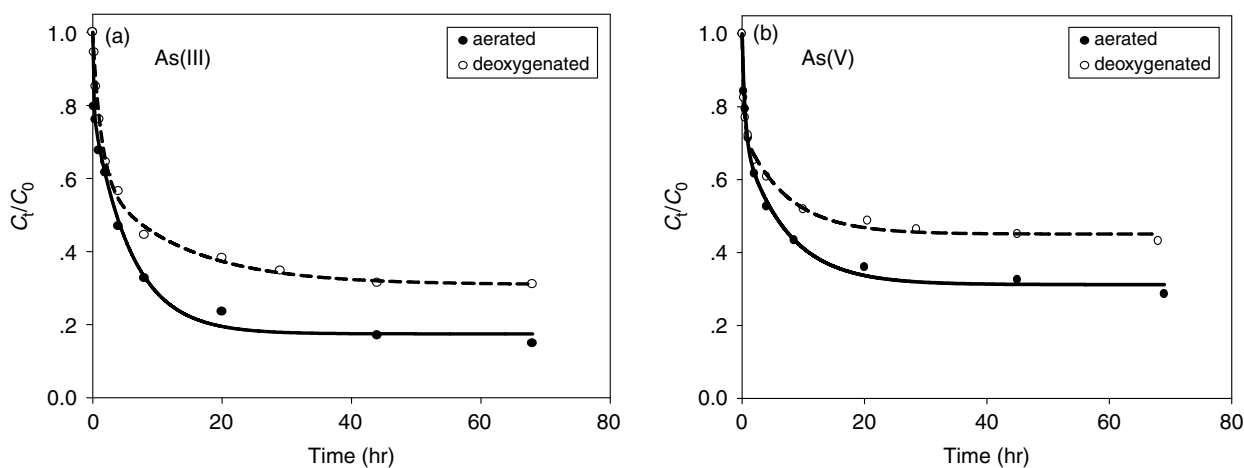


Fig. 5. Fractional (a) As(III) and (b) As(V) adsorption versus time comparing aerobic condition and deoxygenated conditions. Solid lines depicted results of curve-fitting with the biphasic first-order adsorption kinetic model.



Either the amorphous ferric hydroxide (Fe(OH)₃) or maghemite (Fe₂O₃) might be formed on the magnetite surface and cause an increasing specific surface area over time [35,36] and also led to generation of heterogeneous adsorption sites for arsenic. Therefore, this rate-limit process resulted in slow arsenic adsorption kinetics. This process was probably faster in aerated condition with dissolved O₂ than in deoxygenated condition.

Thus, oxidation was likely one of the factors for the observed slow kinetics.

Although surface precipitation was considered as an important factor responsible for the slow process in previous studies [12] where relative high arsenic concentrations were used, it might not be the mechanism for the slow process due to the very low arsenic concentrations involved in the present study. The highest initial concentration of arsenic was 695 μg l⁻¹ (As(V)) for the adsorption kinetics data in Fig. 4. Even a complete adsorption of arsenic on the surface of magnetite nanoparticles occurred, the adsorption would only account for 0.42%

of the total adsorption density (calculated using Visual Minteq based on a surface area of $60 \text{ m}^2 \text{ g}^{-1}$ and a site density of $2.2 \text{ sites nm}^{-2}$). Furthermore, the excellent fit by the DLM model with one surface layer confirmed that surface precipitation could not be the factor that account to the time-dependent adsorption.

4.3. Desorption hysteresis

Fig. 6 shows the desorption results along with adsorption isotherms (15 h) at pH 8.0. For both As(III) and As(V) desorption from magnetite nanoparticles was highly hysteretic. Similar hysteretic desorption has been reported for the desorption of arsenic from mineral oxides and soils, [11,17,19,34] and in the previous studies involving magnetite nanoparticles of different sizes [6,37]. For example, Fuller et al. [9] found that only a small fraction of As(V) desorbed from ferrihydrite in 144 h; they proposed that desorption hysteresis was due to

the slow diffusion within the aggregates of ferrihydrite. Zhang and Selim [14] found that a significant amount of As(V) was irreversibly adsorbed on soils after several repetitive desorption steps, and proposed that desorption hysteresis was due to lack of adsorption/desorption equilibrium resulting from slow diffusion, and/or irreversible adsorption processes involving surface precipitation reactions. Based on the literature studies mentioned above, both slow adsorption and desorption kinetics could have contributed to the observed hysteretic desorption patterns shown in Fig. 6. In particular, the adsorption kinetics data (Fig. 4) indicates that adsorption of As(III) and As(V) can not reach equilibrium after 162 h. Thus, considering the short adsorption time (15 h) involved in the adsorption step, it is possible that adsorption of arsenic continued after desorption was initiated. Note that the mechanisms responsible for the desorption hysteresis are not well understood, and other potentials processes could also result in the hysteretic desorption shown in Fig. 6. For example, Aria and Sparks [34] argued that the increased irreversibility of desorption was possibly caused by the rearrangement of surface complexes and surface precipitation, based on the extended X-ray absorption fine structure (EXAFS) evidence. Undoubtedly, much more studies and further evidence are needed to fully understand the true causes of desorption hysteresis.

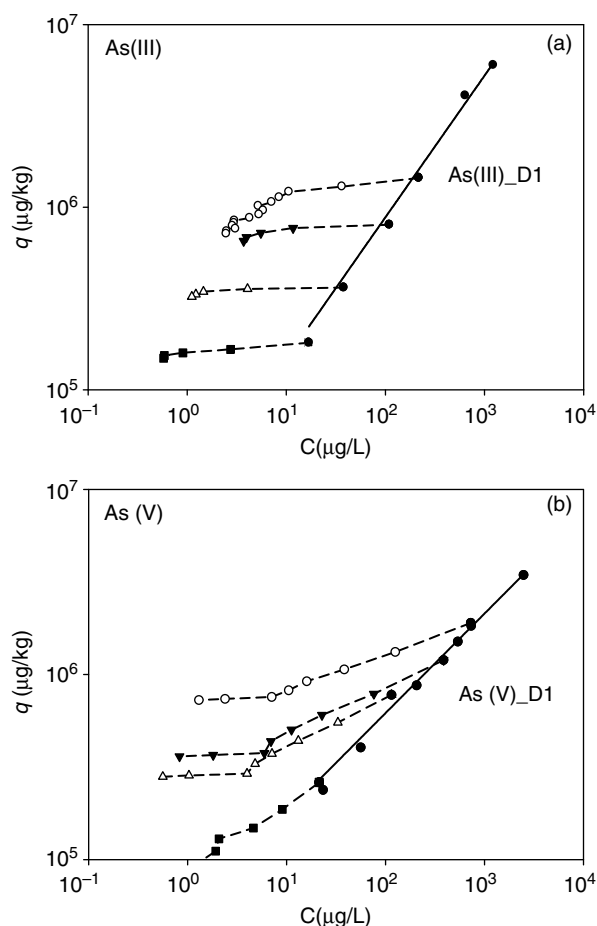


Fig. 6. Adsorption and desorption isotherms of (a) As(III) and (b) As(V) on magnetite nanoparticles. Solid lines represent adsorption isotherms fitted with Freundlich equation. Dotted lines are desorption isotherms initiated from selected points along the adsorption isotherm.

4.4. Modeling of adsorption and desorption using MRM

As shown in Fig. 1 and Eqs. (3)–(5), the MRM accounts for both the nonlinear adsorption equilibrium and slow adsorption kinetics. Therefore, it is possible to quantitatively model both the time-dependent adsorption isotherm data and the biphasic adsorption kinetics data with one set of MRM parameters (i.e., K_e , k_1 , k_2 , k_3 and n). This can be of significant practical importance, because technically it is possible to obtain the five MRM parameters with a small set of data (e.g., one or two adsorption isotherms, or a kinetic data set such as those in Fig. 4) and then use them to predict thermodynamic and kinetic properties for the adsorption/desorption of arsenic on magnetite nanoparticles.

In the present study, the As(III) adsorption isotherm data at different reaction times was used to fit MRM model using the nonlinear least square optimization approach. The fitted model parameters are given in Table 2. As shown in Fig. 3(b), this five-parameter version of MRM was capable of describing the time-dependent adsorption isotherms of As(III) except for the 15 h isotherm. The fact that only one set of model parameters was needed to predict adsorption isotherms at different reaction times (24–120 h) suggested that the applicability of the model is likely independent of adsorption time.

The applicability of the MRM in predicting As(III) adsorption was further tested by comparing the actual adsorption kinetics data in Fig. 4(a) (C_{0-1} and C_{0-2}) with the MRM prediction using the parameters listed in Table 2. Interestingly, the model predictions agreed well with the experimental data, even though the five MRM parameters were obtained by fitting a completely different set of data—the As(III) adsorption isotherms data (Fig. 3). Similarly, the two sets of As(V) adsorption kinetics data (with different initial C_0) in Fig. 4(b) can be well described with one set of the MRM parameters.

Adsorption–desorption data for both As(III) and As(V) was simulated by MRM model based on the optimized parameters from previous adsorption data. Fig. 7 shows the examples for As(III) and As(V) (As(III)_D1 and As(V)_D1), illustrating that MRM model can predict the adsorption–desorption of both As(III) and As(V) quite well. In other words, the simulation on desorption can be easily obtained where one can use parameters based on adsorption data set alone. The three-phase MRM provided good overall description of the adsorption and desorption of arsenic on magnetite nanoparticles.

Although Freundlich model, biphasic first-order model, DLM and MRM can describe the adsorption data of arsenic on magnetite nanoparticles. However, for Freundlich model, the time dependence of K_F implies that the Freundlich model represents an oversimplification of the retention mechanisms on magnetite nanoparticles. The DLM model, a chemical model, is not able to predict the kinetic and even desorption data. Further, many parameters such as surface site density and stability constants may be difficult to obtain, even though they may be chosen from the literature. There is no guarantee

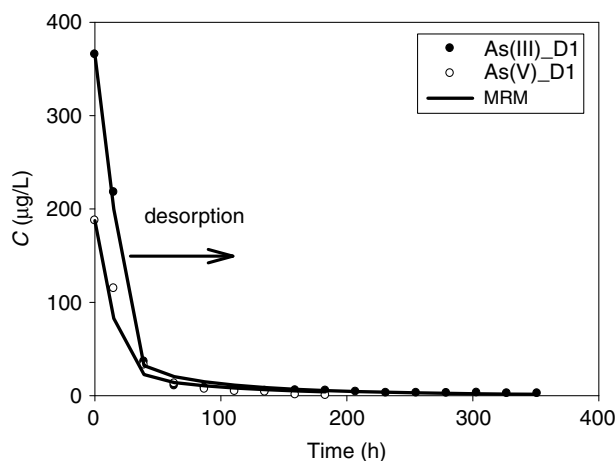


Fig. 7. Comparison of solution concentrations of As(III) and As(V) versus time during adsorption–desorption with the predictions of MRM, using respective one initial concentration for As(III) and As(V) (As(III)_D1 and As(V)_D1) as example.

that such parameters can correctly describe the sorbent. Additionally, the aqueous and surface complexation reaction may become more complex than we expected considering the complexity of solid–electrolyte interface and the plausible heterogeneity of the sorbent (multiple surface sites, different crystal planes, etc.). The excellent fits of adsorption kinetics by biphasic first-order adsorption kinetic model and MRM model is understandable considering the mechanism that two models are based on because the two models take into account both the rapid and slow processes. Nevertheless, biphasic first-order adsorption kinetic model can not be used for a wide range of initial concentration because one set parameters only match with one input concentration. MRM model not only is able to describe the adsorption covered different input concentrations, but also predicts the desorption well based on the adsorption data. Therefore, MRM model is of more practical value and is recommended for predicting the retention of arsenic on nanomagnetite.

5. Conclusions

The adsorption of arsenic on magnetite nanoparticles was time-dependent, exhibited as a biphasic pattern, an initial rapid reaction followed by a much slower reaction. The slow adsorption was not the result of surface precipitation, but might be oxidation of magnetite. Desorption of arsenic on magnetite nanoparticles was hysteretic and should be taken into account in fate and transport modeling and regeneration of magnetite nanoparticles.

Freundlich model, biphasic first-order model, DLM and MRM can describe the adsorption/desorption data of arsenic on magnetite nanoparticles. However, compared to these models, the three-phase MRM provided good overall description of the adsorption and desorption of arsenic on magnetite nanoparticles with different initial concentrations. Therefore, a major implication of this study is that the application of MRM model is recommended in predicting the fate and behavior of arsenic in the water treatment system with magnetite nanoparticles and spread to other iron oxides.

Acknowledgements

This work was supported by National Science Foundation through the Center for Biological and Environmental Nanotechnology (EEC-0118007), Ministry of Education of China (Grant 708020), China-U.S. Center for Environmental Remediation and Sustainable Development, the Key Project of National Natural Science Foundation of China (50830301) and the Fundamental Research Funds for the Central Universities(09QNJJ023).

References

- [1] Arsenic in drinking water seen as threat, US Today, Associated Press (August 2007).
- [2] S.R. Kanel, B. Manning, L. Charlet and H. Choi, Removal of arsenic(III) from groundwater by nanoscale zero-valent iron, *Environ. Sci. Technol.*, 39 (2005) 1291–1298.
- [3] C.T. Yavuz, G.T. Mayo, W.W. Yu, A. Prakash, G.C. Falkner, S. Yean, L. Cong, H.J. Shipley, A.T. Kan, M.B. Tomson, D. Natelson and V.L. Colvin, Low-field magnetic separation of mono-disperse Fe₃O₄ nanocrystals, *Science*, 314 (2006) 964–967.
- [4] V. Chandra, J. Park, Y. Chun, J.W. Lee, I.C. Hwang and K.S. Kim, Water-dispersible magnetite-reduced graphene oxide composites for arsenic removal, *ACS Nano*, 4 (2010) 3979–3986.
- [5] G.Q. Liu, N.R. Liu, H.F. Zhang and L.X. Zhang, The adsorption of arsenic on magnetic iron oxide in aqueous solutions, *Desalination. Water Treat.*, 21 (2010) 96–101.
- [6] S. Yean, L. Cong, C.T. Yavuz, J.T. Mayo, W.W. Yu, J.C. Falkner, A.T. Kan, V.L. Colvin and M.B. Tomson, Effect of magnetite particle size on adsorption and desorption and arsenate, *J. Mater. Res.*, 20 (2005) 3255–3264.
- [7] H.J. Shipley, S. Yean, A.T. Kan and M.B. Tomson, Adsorption of arsenic to magnetite nanoparticles: effect of particle concentration, pH, ionic strength, and temperature, *Environ. Toxicol. Chem.*, 28 (2009) 509–515.
- [8] W. Yang, A.T. Kan, W. Chen and M.B. Tomson, pH-dependent effect of zinc on arsenic adsorption to magnetite nanoparticles, *Water Res.*, 44 (2010) 5693–5701.
- [9] C.C. Fuller, J.A. Davis and G.A. Waychunas, Surface chemistry of ferrihydrite: part 2. Kinetics of arsenate adsorption and coprecipitation, *Geochim. Cosmochim. Acta*, 57 (1993) 2271–2282.
- [10] K.P. Raven, A. Jain and R.H. Loeppert, Arsenite and arsenate adsorption on ferrihydrite: kinetics, equilibrium and adsorption envelopes, *Environ. Sci. Technol.*, 32 (1998) 344–349.
- [11] S.E. O'Reilly, D.G. Strawn and D.L. Sparks, Residence time effects of arsenate adsorption/desorption mechanisms on goethite, *Soil Sci. Soc. Am. J.*, 65 (2001) 67–77.
- [12] H. Zhao and R. Stanforth, Competitive adsorption of phosphate and arsenate on goethite, *Environ. Sci. Technol.*, 35 (2001) 4753–4757.
- [13] L.E. Williams, M.Q. Barnett, T.A. Kramer and J.G. Melville, Adsorption and transport of arsenic (V) in experimental subsurface systems, *J. Environ. Qual.*, 32 (2003) 841–850.
- [14] H. Zhang and H.M. Selim, Kinetics of arsenate adsorption-desorption in soils, *Environ. Sci. Technol.*, 39 (2005) 6101–6108.
- [15] H. Zhang and H.M. Selim, Modeling the transport and retention of arsenic(V) in soils, *Soil Sci. Soc. Am. J.*, 70 (2006) 1677–1687.
- [16] P.R. Grossl, M. Eick, D.L. Sparks, S. Goldberg and C.C. Ainsworth, Arsenate and chromate retention mechanisms on goethite, 2. Kinetic evaluation using a pressure-jump relaxation technique, *Environ. Sci. Technol.*, 31 (1997) 321–326.
- [17] J. Zhang and R. Stanforth, Slow adsorption reaction between arsenic species and Goethite (α-FeOOH): Diffusion or heterogeneous surface reaction control, *Langmuir*, 21 (2005) 2895–2901.
- [18] C. Luengo, M. Brigante and M. Avena, Adsorption kinetics of phosphate and arsenate on goethite, A comparative study, *J. Colloid Interface Sci.*, 311 (2007) 354–360.
- [19] Z. Lin and R.W. Puls, Adsorption, desorption and oxidation of arsenic affected by clay minerals and aging process, *Environ. Geol.*, 39 (2000) 753–759.
- [20] B.J. Lafferty and R.H. Loeppert, Methyl arsenic adsorption and desorption behavior on iron oxides, *Environ. Sci. Technol.*, 39 (2005) 2120–2127.
- [21] M. Quaghebeur, A. Rate, Z. Rengel and C. Hinz, Desorption kinetics of arsenate from kaolinite as influenced by pH, *J. Environ. Qual.*, 34 (2005) 479–486.
- [22] Y. Masue, R.H. Loeppert and T.A. Kramer, Arsenate and arsenite adsorption and desorption behavior on coprecipitated aluminum: iron hydroxides, *Environ. Sci. Technol.*, 41 (2007) 837–842.
- [23] H. Genç-Fuhrman, J.C. Tjell and D. McConchie, Adsorption of arsenic from water using activated neutralized red mud, *Environ. Sci. Technol.*, 38 (2004) 2428–2434.
- [24] X. Wen, Q. Du and H. Tang, Surface complexation model for the heavy metal adsorption on natural sediment, *Environ. Sci. Technol.*, 32 (1998) 870–875.
- [25] J.P. Gustafsson, Visual MINTEQ version 2.53 (2005).
- [26] M.C. Amacher, H.M. Selim and I.K. Iskandar, Kinetics of chromium(VI) and cadmium retention in soils—a nonlinear multi-reaction model, *Soil Sci. Soc. Am. J.*, 52 (1988) 398–408.
- [27] M.C. Amacher, H.M. Selim and I.K. Iskandar, Kinetics of mercuric chloride retention by soils, *J. Environ. Qual.*, 19 (1990) 382–388.
- [28] H.M. Selim and D.L. Sparks, Heavy metals release in soils. CRC Lewis, Boca Raton, FL (2001).
- [29] L.O. Jay, Inexact simplified Newton iterations for implicit Runge-Kutta methods, *SIAM J. Numer. Anal.*, 38 (2001) 1369–1388.
- [30] G. Morin, G. Ona-nguema, Y. Wang, N. Menguy, F. Juillot, O. Proux, F. Guyot, G. Calas, J.G. Brown and G.E. Brown Jr, Extended X-ray absorption fine structure analysis of arsenite and arsenate adsorption on maghemite, *Environ. Sci. Technol.*, 42 (2008) 2361–2366.
- [31] S. Dixit and J.G. Hering, Comparison of arsenic(V) and arsenic(III) sorption onto iron oxide minerals: implications for arsenic mobility, *Environ. Sci. Technol.*, 37 (2003) 4182–4189.
- [32] N. Marmier, A. Delisée and F. Fromage, Surface complexation modeling of Yb(III), Ni(II), and Cs(I) sorption on magnetite, *J. Colloid Interface Sci.*, 211 (1999) 54–60.
- [33] H. Guo, D. Stüben and Z. Berner, Adsorption of arsenic(III) and arsenic(V) from groundwater using natural siderite as adsorbent, *J. Colloid Interface Sci.*, 315 (2007) 47–53.
- [34] Y. Arai and D.L. Sparks, Residence time effect on arsenate surface speciation at the aluminum oxide–water interface, *Soil Sci.*, 167 (2002) 303–313.
- [35] V.S. Coker, A.G. Gault, C.I. Pearce, G. Van Der Laan, N.D. Telling, J.M. Charnock, D.A. Polya and J.R. Lloyd, XAS and XMCD evidence for species-dependent partitioning of arsenic during microbial reduction of ferrihydrite to magnetite, *Environ. Sci. Technol.*, 40 (2006) 7745–7750.
- [36] R.M. Cornell and U. Schwertmann, The iron oxides: structure, properties, reactions, occurrences and uses. Wiley-VCH, New York (1996).
- [37] J.T. Mayo, C.T. Yavuz, S. Yean, L. Cong, H.J. Shipley, W. Yu, J.C. Falkner, A.T. Kan, M.B. Tomson and V.L. Colvin, The effect of nanocrystalline magnetite size on arsenic removal, *Sci. Technol. Adv. Mater.*, 8 (2007) 71–75.